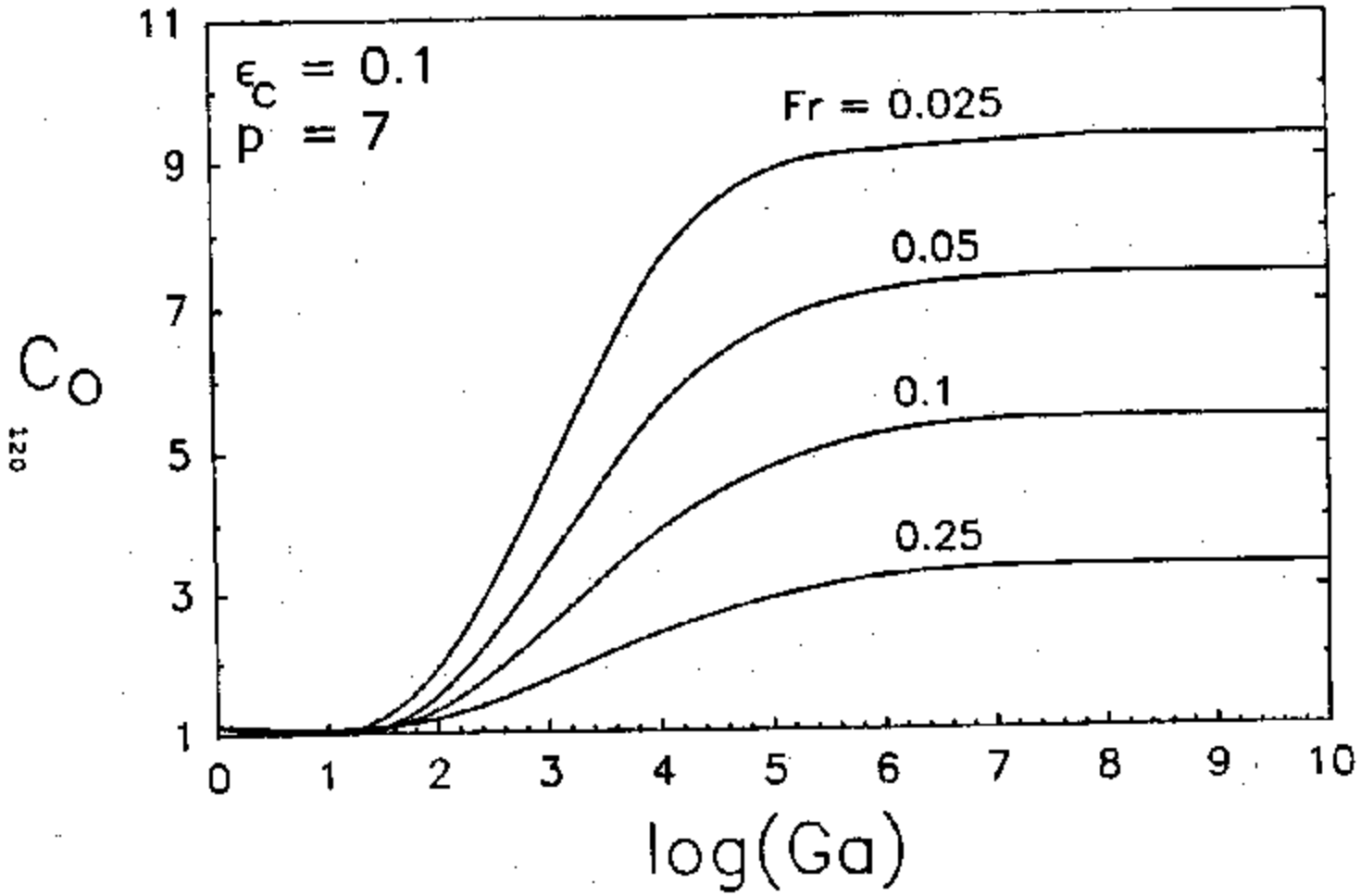

Figure 2.80. Profile constant C_o for various Fr and Ga for void distributions given by [1] with ϵ_c = 0.1 and p = 7. The comments on Fr and Ga in the legend to figure 2.74 apply.

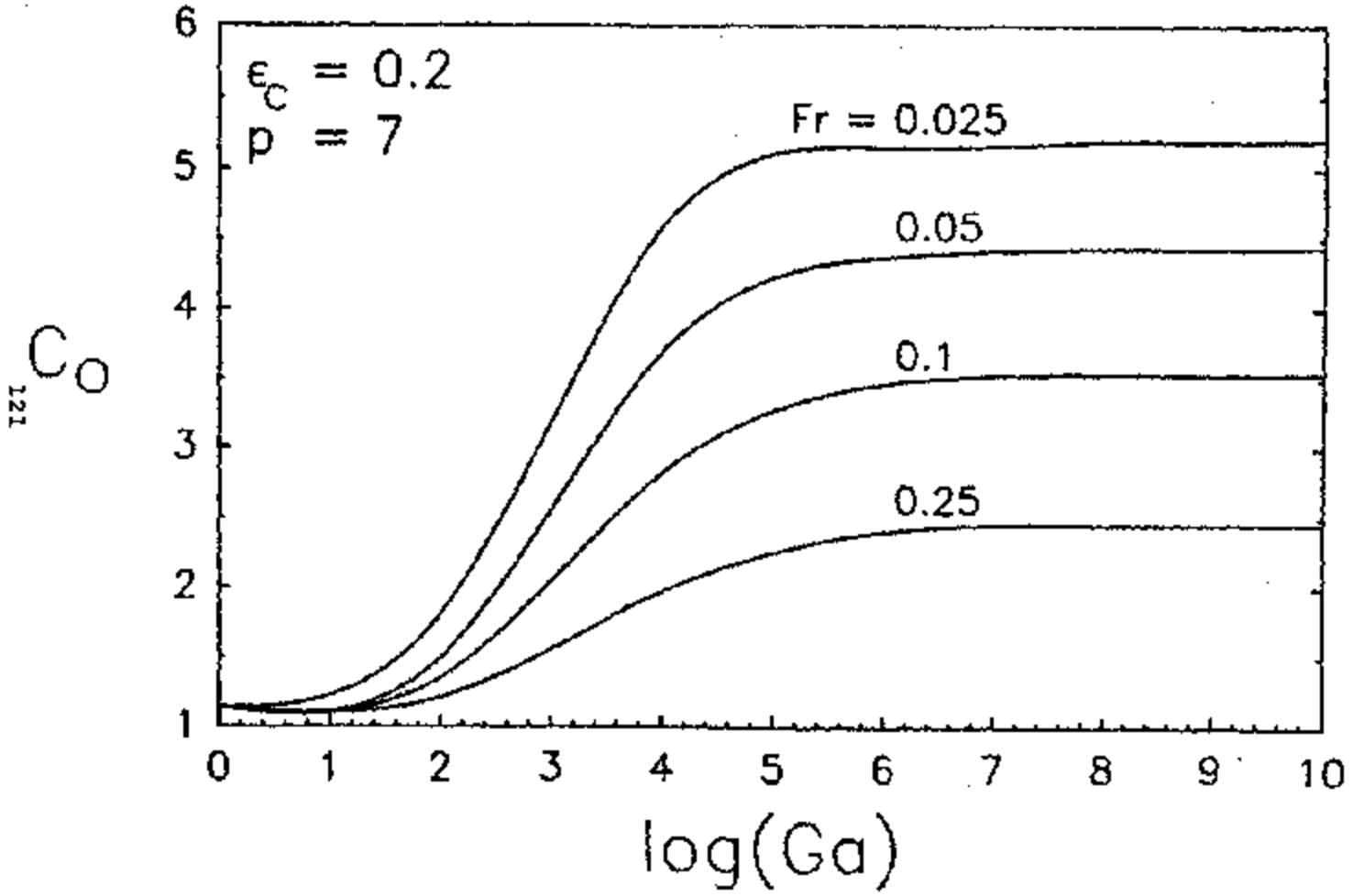

Figure 2.81. Profile constant C_0 for various Fr and Ga for void distributions given by [1] with ϵ_c = 0.2 and p = 7

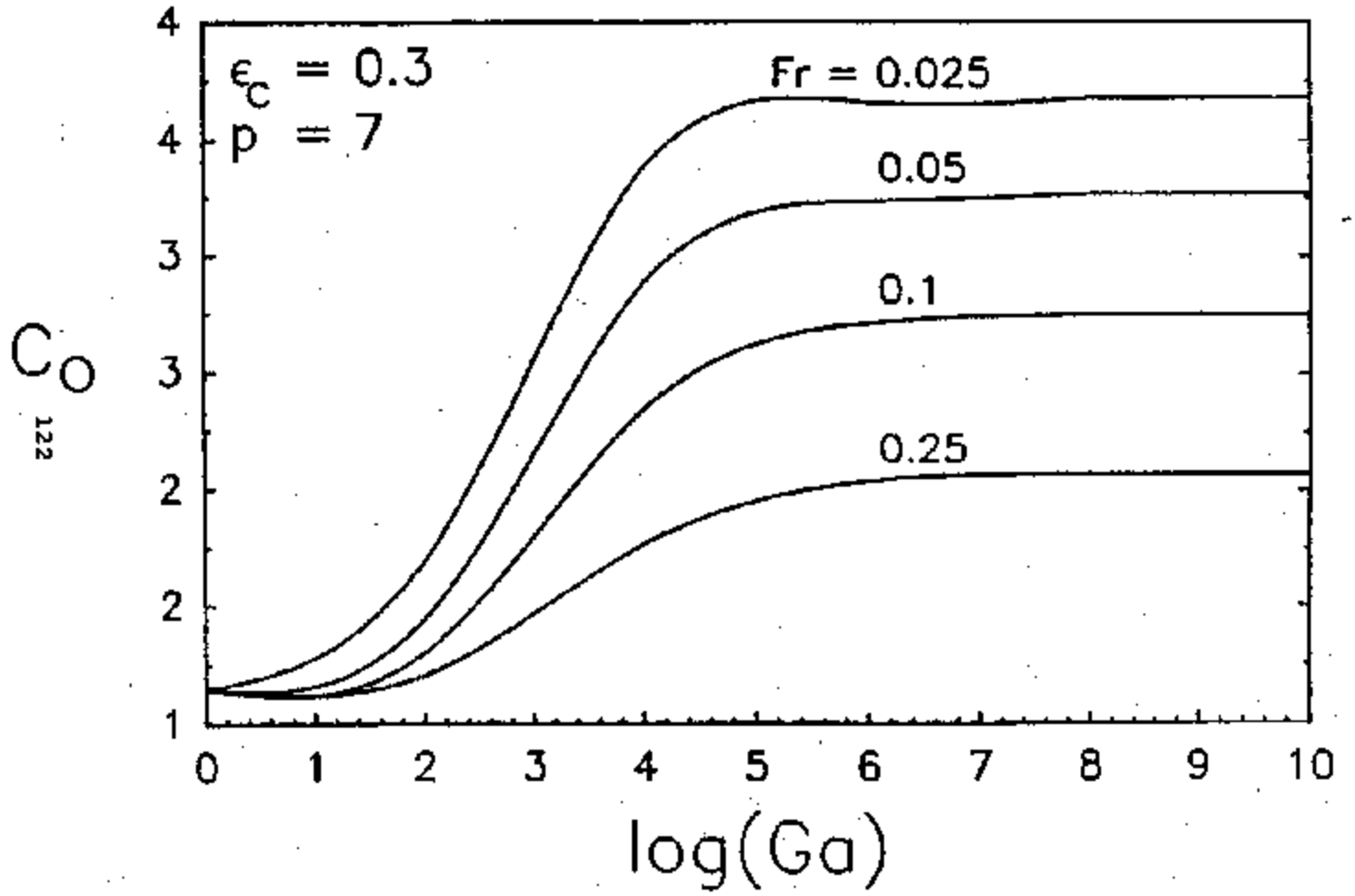

Figure 2.82. Profile constant C_0 for various Fr and Ga for void distributions given by (1) with $\epsilon_c = 0.3$ and $p = 7$.

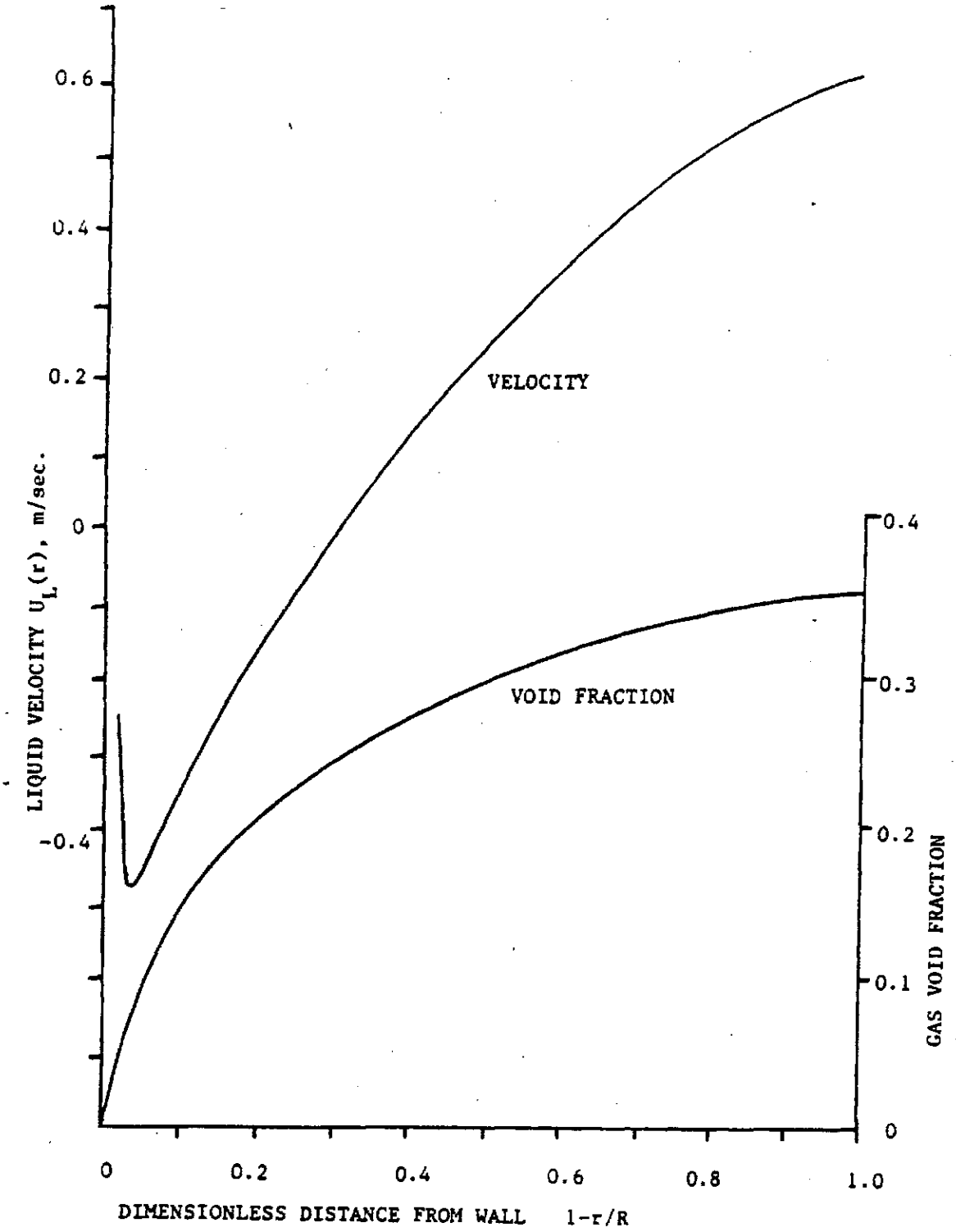

Figure 2.83. Void profile from the data of Hills (15.2 cm dia column, air superficial velocity 169 mm/s) and the sympathetic liquid velocity profile, found using themethod of Clark *et al.* (1987). It is evident that the flow is buoyancy-driven.

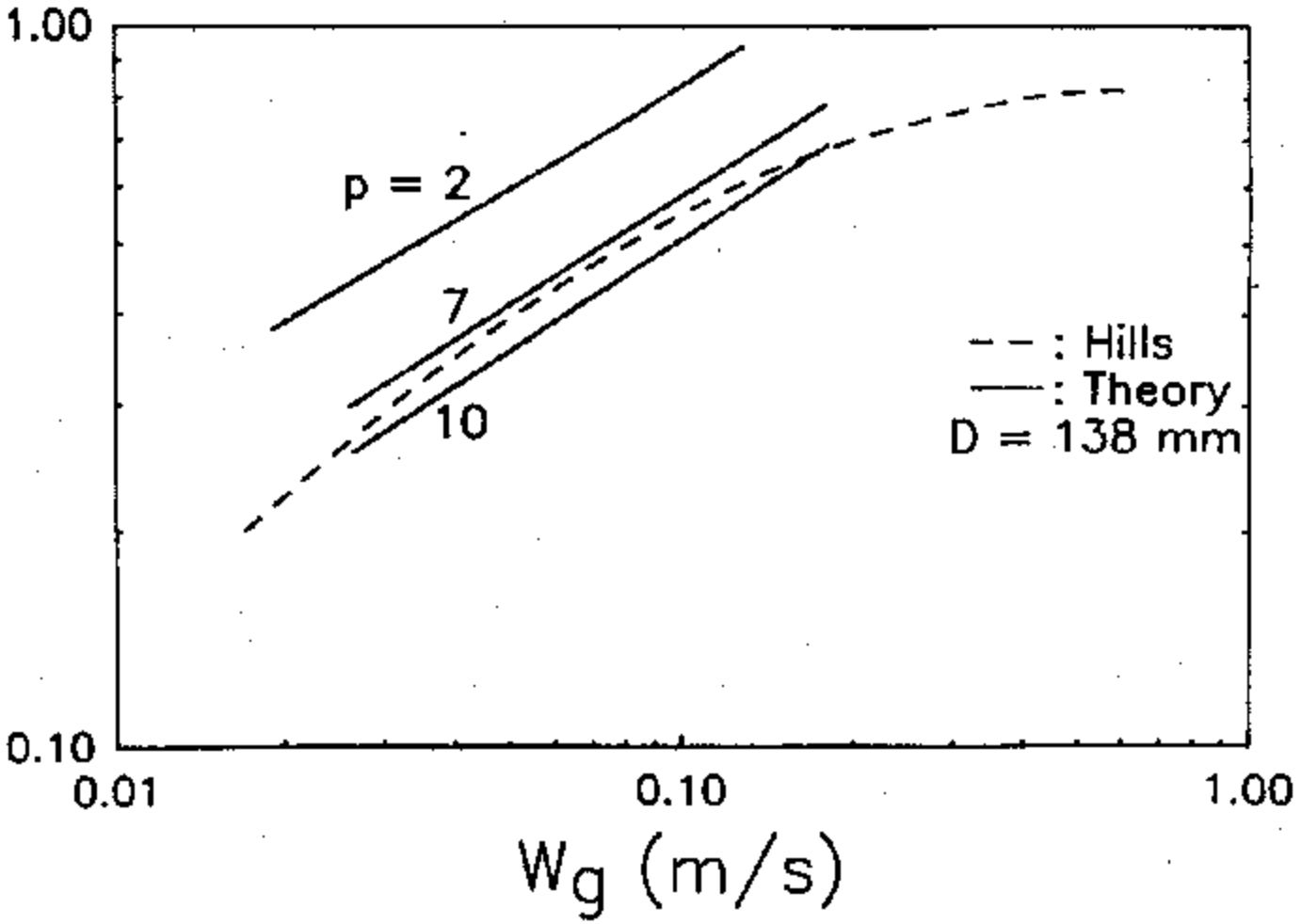

Figure 2.84. The model was used to predict the centerline liquid velocity in the column when there was no net liquid flow for various gas flowrates and values of the void distribution parameter, p. (Note that ε_c can be found given p, W_g and the velocity across the column.) Hills' measured values of centerline velocity are close to the predicted lines for values of p = 7 to 10. At very high gas flowrates the mixture properties and behavior will deviate significantly from those of the liquid phase, causing error in the predictions using the present model.

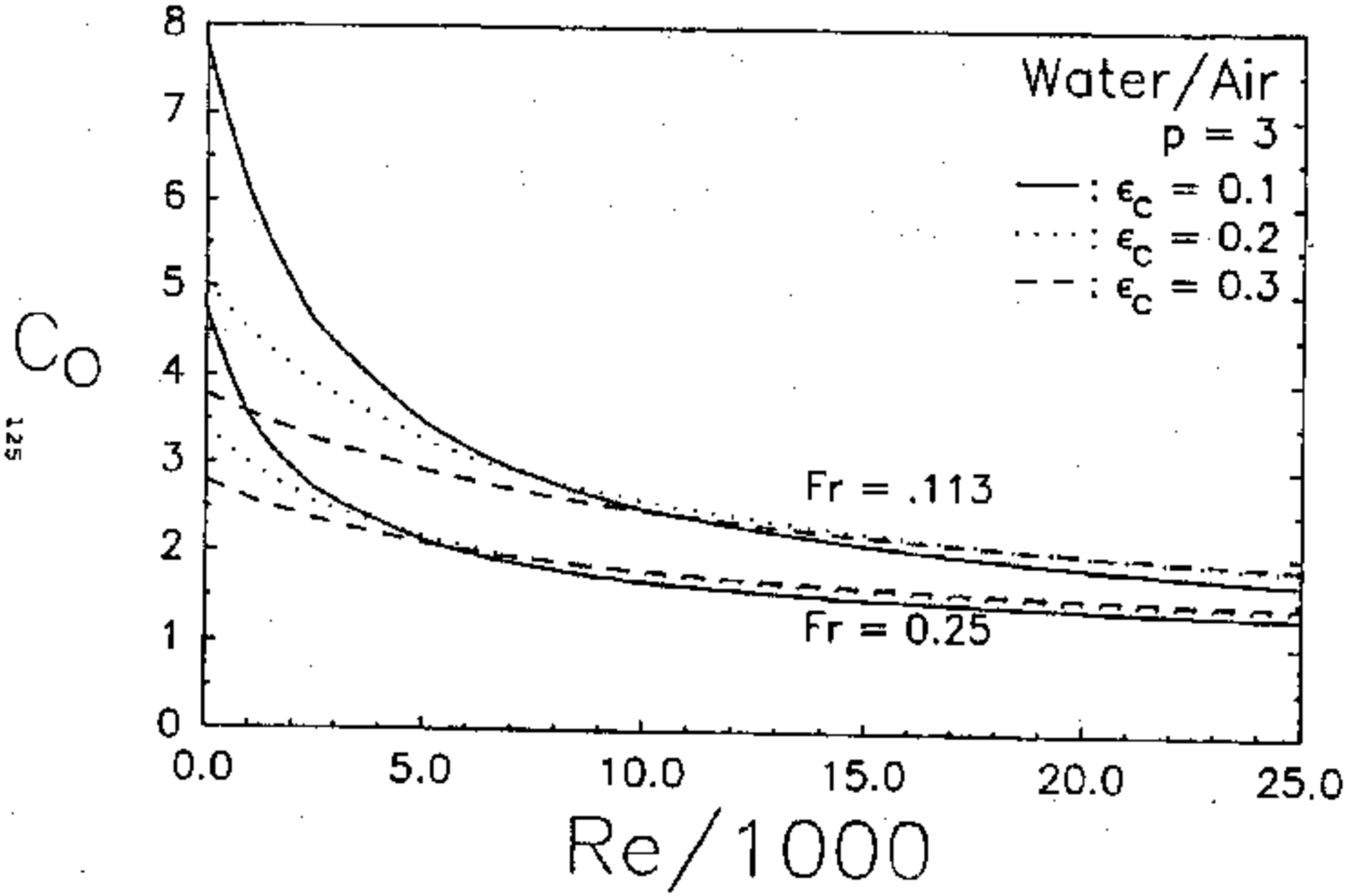

Figure 2.85. The profile constant, C_o, was calculated for the case where there was a net upflow in the column (represented by the liquid flow Re = $\rho UD/\mu$) but when buoyancy effects were still significant. Fr = 0.25 corresponds to a bubble rise velocity of 250 mm/s in a 100 mm dia pipe, and Fr = 0.113 for a 500 mm dia pipe.

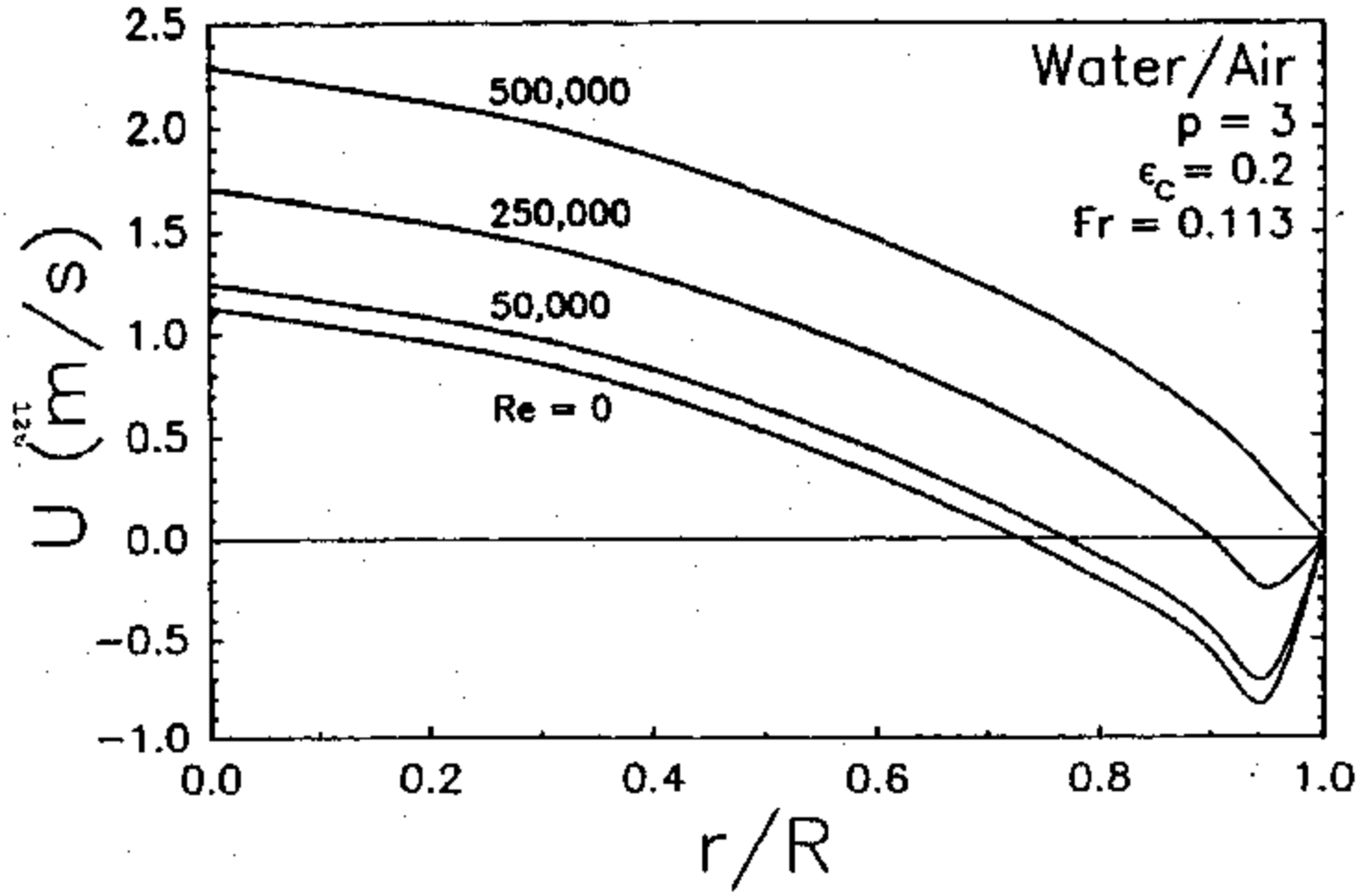

Figure 2.66. Axial liquid velocity profiles for the case of a 500 mm dia bubble column (Re = 0) and pipe carrying a two-phase upflow (Re > 0), when the void fraction is greatest at the center.

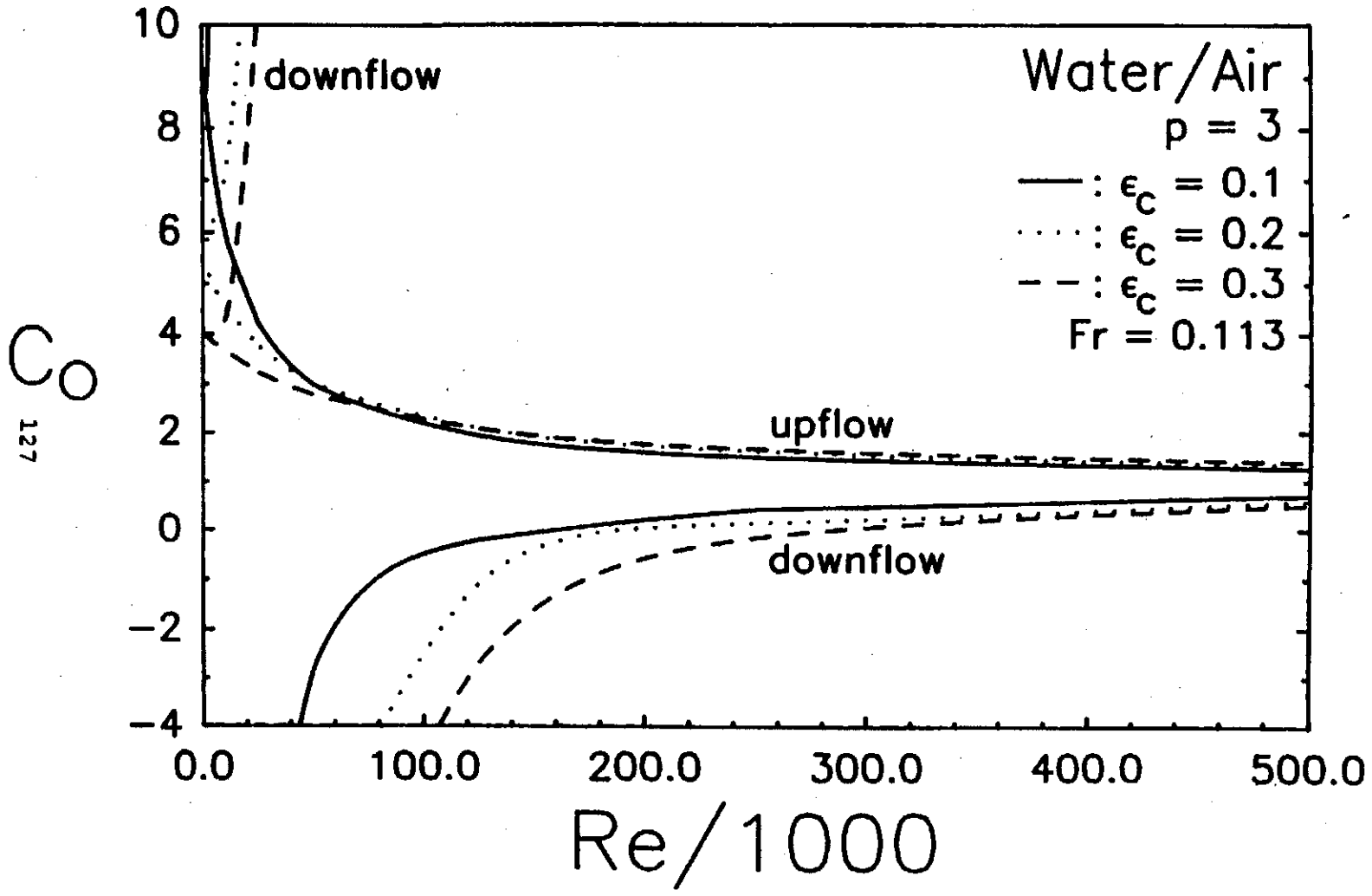

Figure 2.87. A plot yielding values of C_o, for upflow and downflow, in a 500 mm pipe with the void fraction having a maximum at the pipe center. Note the choking condition for the downflow case, where C_o assumes very high values; this is when the bubbles cannot rise upward through the downflow, and when the downflow velocity is not strong enough to carry them downward.

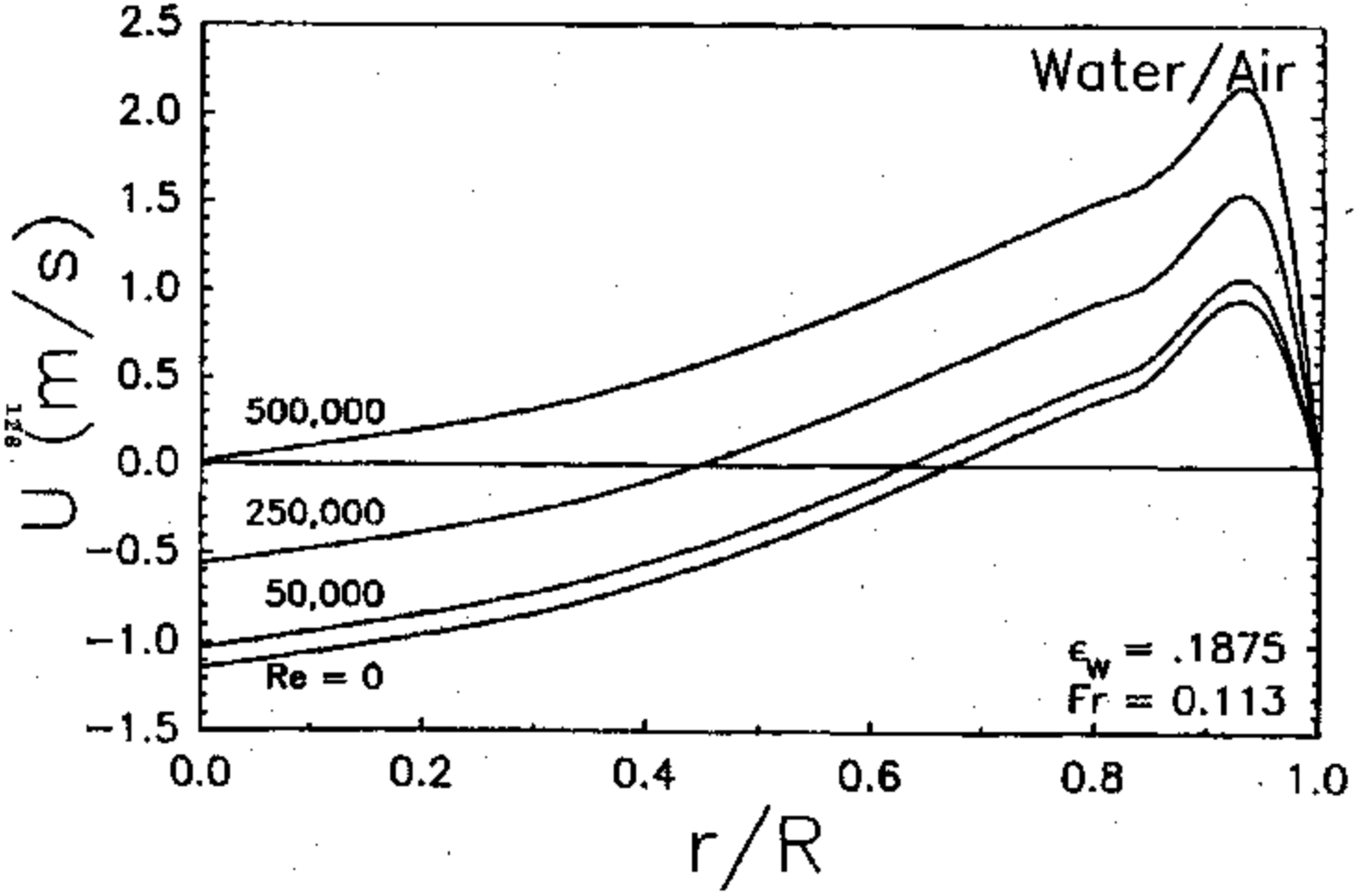

Figure 2.88. When the bubbles are concentrated in an annular region, buoyancy forces and wall effects are in competition during two-phase upflow. For this case in a 500 mm dia pipe, liquid flow is downward at the center for net upflow Re < 500,000. The void profile used to generate this plot is given in figure 2.89.

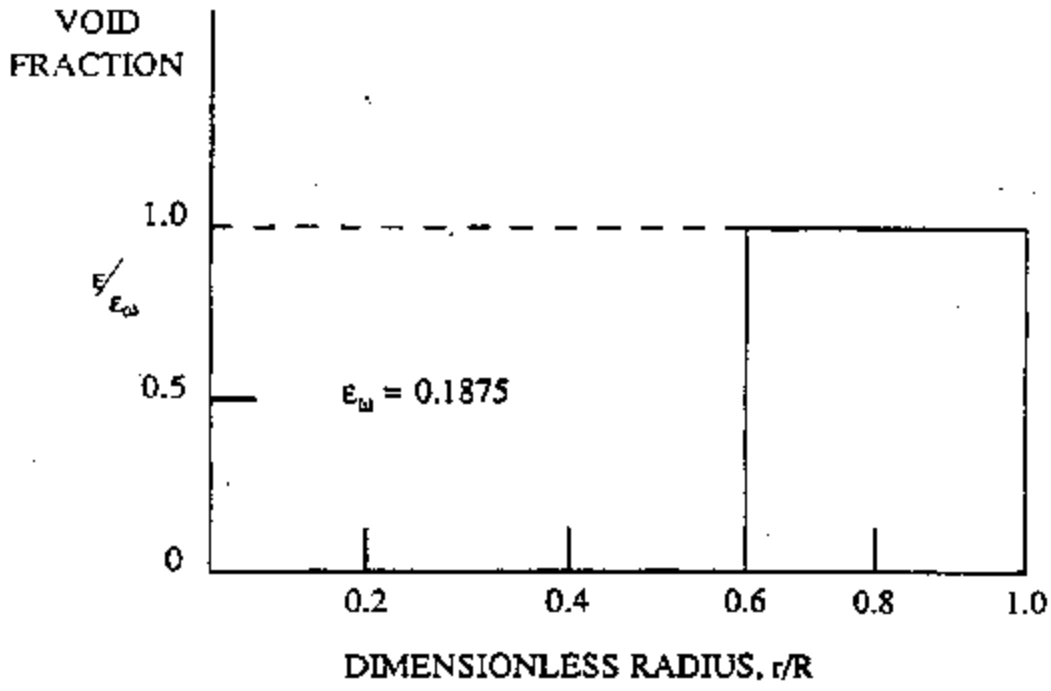

Figure 2.89. This annular void distribution, intended to imitate saddle-shaped distributions observed by some previous researchers, was used to generate the velocity profiles shown in figure 2.88.

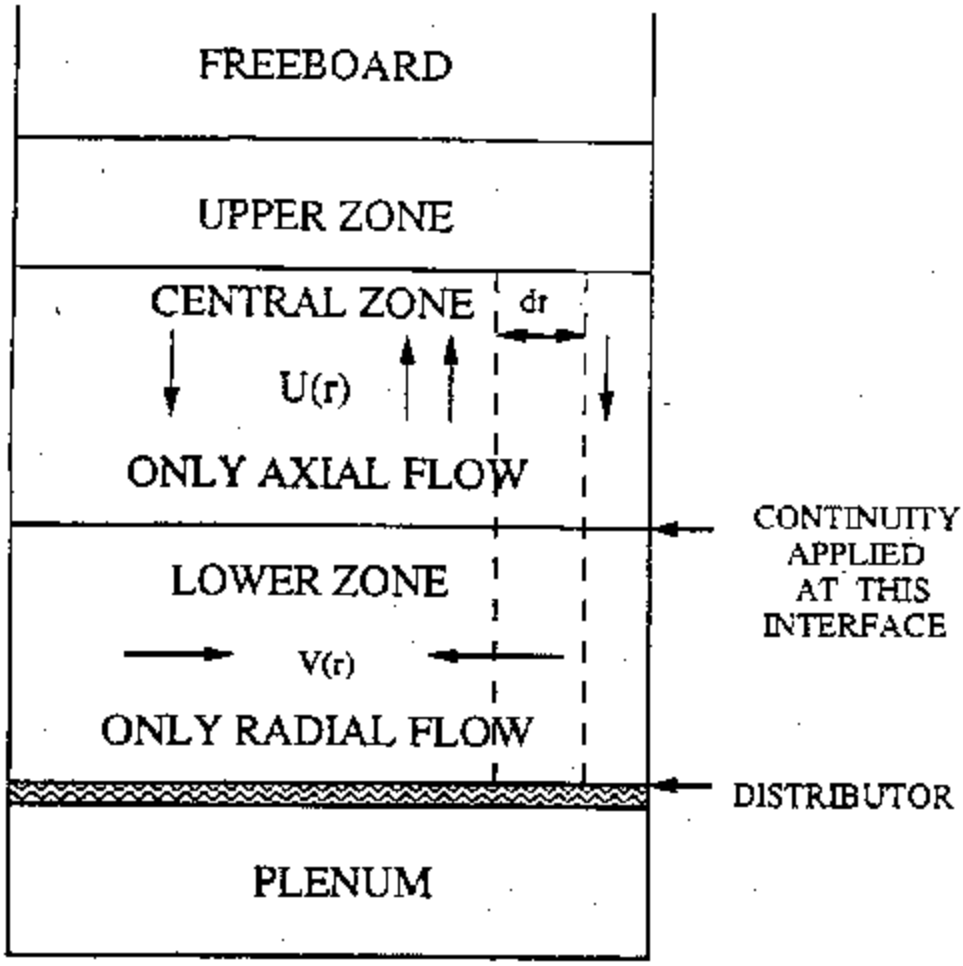

Figure 2.90. To model radial bubble motion, a two-zone, one-dimensional approach was used. In the central zone, all fluid motion was considered axial. In the lower zone, all liquid motion was considered radial. Bubbles rising vertically through the radial field were moved inward. In this way an uneven void distribution can develop although gas introduction through the distributor may be even.

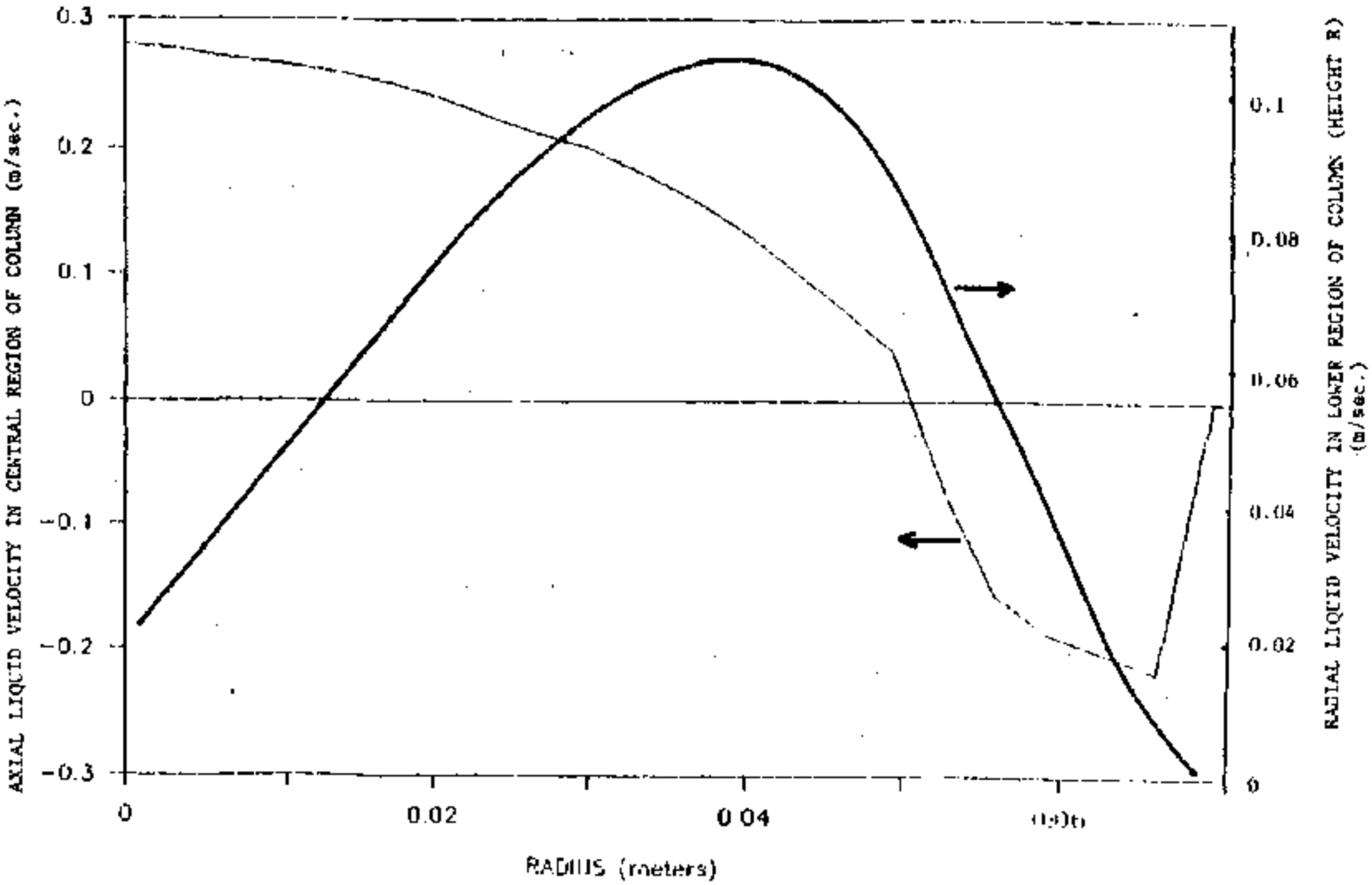

Figure 2.91. Distribution of radial velocity in the lower zone (√) and axial velocity in the center zone (U), corresponding to Hills' air-water column, with an air superficial velocity of 38 mm/s.

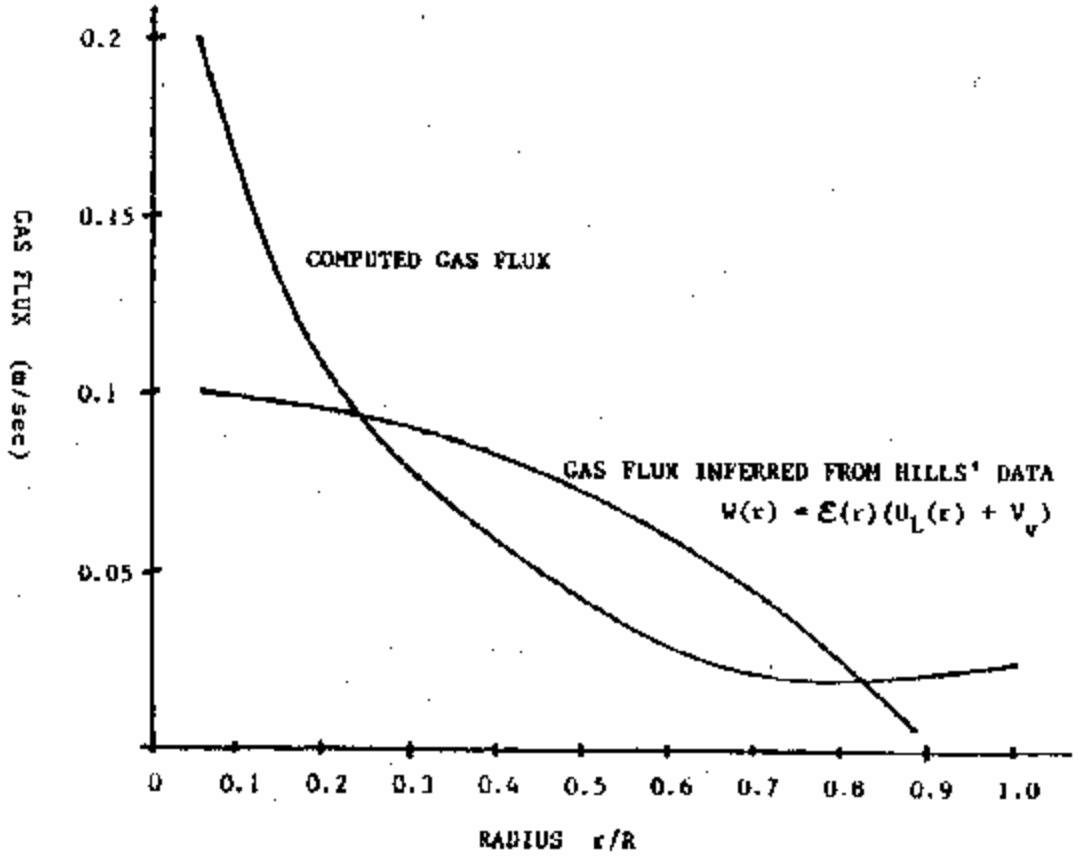

Figure 2.92. The gas flux, $W(r)$, computed from bubble motion in the lower zone, is compared here with the $W(r)$ found from the product of $\varepsilon(r)$ and $(U_L)(r)$ are given in Hills' paper.